Characterization of Cementitious Materials Exposed to Freezing and Thawing using 3D Scans

Alexander Haynack[a,*], Jithender J. Timothy[a], Thomas Kränkel[a] and Christoph Gehlen[a]

[a]*Technical University of Munich; TUM School of Engineering and Design, Department of Materials Engineering, Chair of Materials Science and Testing; Centre for Building Materials (cbm) Munich, Franz-Langinger-Straße 10, Munich 81245, Germany*

ARTICLE INFO

Keywords:
cementitious materials
concrete
mortar
freeze-thaw resistance
durability
3D-scan
Python

ABSTRACT

Deterioration of concrete subjected to freezing and thawing climatic conditions is one of most important factors affecting the durability of concrete infrastructure in cold climates. The freeze-thaw resistance of cementitious materials like concrete and mortar can be determined by the CDF test (Capillary Suction of De-icing chemicals and Freeze-Thaw Test). Here, concrete specimens are subjected to repeated freeze-thaw cycles with simultaneous addition of de-icing salt and the amount of material weathered near the surface is determined. For concretes with adequate freeze-thaw resistance, this test method works very well. However, specimens with inadequate or unknown performance often experience increased edge weathering, which is caused by the detachment of the lateral isolation tape. The increasing edge influence thus leads to a falsification of the results and consequently to an underestimation of the actual freeze-thaw resistance of the material. In materials research in particular, however, concretes with high levels of weathering are studied in order to be able to investigate various factors of influence on the freeze-thaw resistance of concretes in a targeted manner. This paper presents a novel methodology that delivers new information regarding the weathering of CDF test samples and the associated distribution function of the height decrease using high resolution 3D scan data. The results indicate a correlation between the progression of the distribution function and the sample's maximum aggregate size. The change of the sample volume can be used to support the weathering results of the standard CDF methodology. The increase of the surface area is used to estimate the tortuosity of the sample surface. It indicates an asymptotic curve approaching a specific maximum value, which is dependent on the the weathering depth of the sample.

1. Introduction

By 2050, 70 % of the world's population is expected to live in urban areas [1]. For this reason, huge investments in concrete infrastructure will be required. Improving the sustainability of concrete infrastructure is currently of utmost importance. Extending the service life of concrete infrastructure is one of the most important components to improve sustainability. Frost damage is an important factor affecting the durability of concrete in cold climates [2], e.g. damage to concrete pavements caused by freezing during winter. Such damages are mainly initiated by moisture transport into the concrete. Transport processes in concrete largely depend on the distribution, amount, type, size, and shape of the capillary pores within the system [3]. The formation of these pores is caused by excess water, which is not used for the hydration process and therefore bound neither chemically nor physically. The resulting capillary pore structure enables the intrusion of gases and liquids into the concrete [4].

Deterioration induced by exposing the material to freezing and thawing loads, can be categorized into weathering of the surface and internal microcracking. Figure 1 shows the surface deterioration of a concrete wall with a high saturation freezing and thawing exposure at a floodgate in Germany. The 10 year old building, composed of a CEM III/A, shows several freeze-thaw induced surface damages in the water splash zone.

Figure 1: Surface deterioration of a concrete wall with a high saturation freezing and thawing exposure at a floodgate in Germany.

Fundamental contributions to our current understanding of freeze-thaw-induced deterioration of cement-based materials include the work of Setzer (thermal equilibrium / micro-ice-lens model) [5], Powers and Helmuth (osmotic pressure) [6], Coussy and Monteiro (poromechanics) [7], Scherer (crystallization pressure) [8, 9], Zhao (nanofluidic salt inclusions) [10] and [11]. These theories formed the basis for the development of a variety of analytical and

*This document is the results of the research project funded by the German Research Foundation (DFG), project number 428338963.

*Corresponding author
alexander.haynack@tum.de (A. Haynack); jithender.timothy@tum.de (J.J. Timothy); thomas.kraenkel@tum.de (T. Kränkel); gehlen@tum.de (C. Gehlen)
ORCID(s): 0000-0003-2262-6111 (A. Haynack); 0000-0002-1975-6524 (J.J. Timothy); 0000-0002-5650-3825 (T. Kränkel); 0000-0002-1214-3960 (C. Gehlen)

Preprints (www.preprints.org) | NOT PEER-REVIEWED | Posted: 28 November 2022 doi:10.20944/preprints202211.0507.v1

Table 1
Preconditioning and composition of mortar samples.

Label	Preconditioning	W/C	Cement kg/m³	Water kg/m³	Aggregates kg/m³	Max. aggr. size mm
M1 20-65	20 °C, 65 % r.H.	0.55	560	308	1312	2
M1 WS	water storage	0.55	560	308	1312	2
M2 20-65	20 °C, 65 % r.H.	0.55	730	401.5	932	0.5

computational models for model-based characterization of freeze-thaw induced damage to cementitious materials. An accurate characterization of the deterioration process will potentially improve our current understanding of the deterioration mechanisms.

The CDF test is considered as the standard test method for determining the freeze-thaw resistance of concrete in Germany. Here, the concrete or mortar specimens are cyclically exposed to temperatures from 20 to -20 °C over the course of twelve hours. This so called freeze-thaw cycle is repeated 28 times. The decisive test criterion is the weathering of the sample surface. For isolation purposes and a guaranteed one-dimensional freeze-thaw exposition, the specimens are sealed with aluminum laminated butyl rubber film [12]. Concrete mixtures with high weathering cause the isolation to scale off which results in a two-dimensional exposition and an increased weathering in the peripheral areas of the specimens, see figure 2.

Figure 2: CDF sample showing the detachment of the isolation tape.

The use of 3D scanning technology has already been proven in the field of mechanical engineering [13, 14, 15, 16]. It is mainly used for quality control and reverse engineering by comparing scan data with their respective digital models. As a result, the scan-to-model differences such as weld joints, deformations, and other deviations are detected and analyzed [16]. The idea of this target-actual comparison is applied to the field of damage assessment of concrete after freeze-thaw and de-icing salt induced expositions. For this, the test samples are scanned after certain freeze-thaw cycles and afterwards aligned to a reference scan before freeze-thaw exposition. This allows the detection of the surface weathering and degradation caused by repeated freeze-thaw cycles. The problem of isolation tape scaling can also be countered with this methodology by simply removing the peripheral areas of the sample (see figure 3) and therefore excluding it from the analysis.

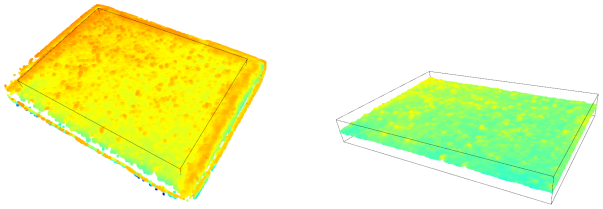

(a) (b)

Figure 3: Sample surface before (a) and after (b) removal of the peripheral areas.

The device used for this study is the HandySCAN Black Elite by Creaform [17]. It shows an accuracy of 25 µm, which has been confirmed by calibration measurements prior to this study. The hand-held design of the device delivers a high performance and a great suitability for the presented problem formulation.

At first, the used mix designs and applied preconditionings are presented in the following chapter. Afterwards, the standardized CDF test methodology is described shortly. The main focus of this paper lies on the description of the development of the 3D scan alignment algorithm and the consequent data analysis. Finally, the results are presented and discussed.

2. Materials

The mix designs used in this study consist of a Portland cement CEM I 42.5N with a maximum aggregate size of either 2 mm (M1) or 0.5 mm (M2). Both mixtures had a w/c ratio of 0.55 and were held in the framework for 1 day. After the removal of the framework, the samples were stored under water until the sample age of 7 days. Subsequently, the mortar samples were stored in standard climate conditions of 20 °C and 65 % relative humidity for 21 days until the sample age of 28 days according to [12]. Additionally, another set of samples from mixture M1 has been stored completely under water before testing. One set of samples consists of 5 individual mortar samples with the dimensions of 15x11x7 cm³. The applied preconditioning and the composition of the sample sets used in this study are given in table 1.

Preprints (www.preprints.org) | NOT PEER-REVIEWED | Posted: 28 November 2022 doi:10.20944/preprints202211.0507.v1

3. CDF

After reaching the sample age of 28 days, the samples were put into the CDF containment boxes for capillary saturation for 7 days. Here, the sodium chloride testing solution can be absorbed by the samples. After that, the cyclical freeze-thaw exposition from 20 °C to -20 °C is started for a total duration of 14 days. This complies to 28 freeze-thaw cycles (FTC). For further information regarding the standard CDF test, please refer to [12].

4. 3D-Scan data

4.1. Overview

Parallel to the CDF test, the mortar samples are scanned after 0, 4, 10, 14, 18, 24, and 28 FTC. Figure 4 shows an exemplary setup for the process of sample scanning. The freeze-thaw exposed testing surface and the back side of the sample are both scanned with the 3D scanner, see figure 4 (a). Prior to scanning, the sample is positioned on top of a 3D-printed scanning template, which is equiped with target markers. These markers are required by the scanner for orientation and generation of the coordinate system of the point cloud, see figure 4 (b).

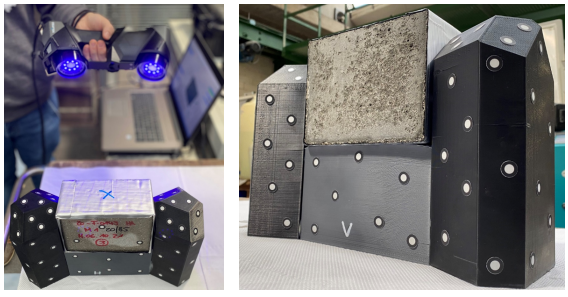

(a) (b)

Figure 4: 3D scanning setup: (a) scanning procedure showing the 3D hand-held device scanning the mortar specimen, (b) specimen placed in the mounting bracket covered in white target markers.

The following sections describe the processes of the novel methodology in detail.

4.2. Scan data alignment process

The data obtained from the 3D-Scanner is a point cloud i.e. list of co-ordinates specified in three dimensional space with the corresponding normals. The normal vector is used to obtain an orientation of the surface that comprises the neighborhood of a certain point. In our case, for a given specimen, we have a series of point-clouds corresponding to the state of the weathered surface after being subjected to a certain number of freeze-thaw cycles. In order to evaluate the relative changes to the specimen, we have to compare the scans. Given the point-cloud data of two scans corresponding to two different states of weathering, the point-cloud data can be compared only if the reference co-ordinate system is the same in both cases. However this is not the case. Manually ensuring the origin of the co-ordinate system is aligned for all subsequent scans corresponding to the level of weathering is cumbersome and not accurate. Thus we have used a computational technique to align the scans.

The strategy to automatically align scans pertaining to a certain specimen at various levels of weathering is as follows. Firstly it is assumed that there is a surface region in the scan that is not weathered and whose surface characteristics such as pores and other geometrical artifacts remain constant throughout the freeze-thaw loading process. Typically this can be the surface that is not in contact with the solution. A representative planar section of this surface is first extracted from all the scans that correspond to the same specimen. Subsequently, a transformation matrix that aligns this surface is computed using an point-set registration algorithm. This transformation matrix is then applied to the complete point cloud to obtain the final alignment. While the point-set registration procedure is a major component of the algorithm, additional pre-processing and post-processing algorithms are required for the alignment due to the noise and the missing correspondences between the pairs of point clouds that have to be aligned.

Each alignment procedure involves two point clouds. A source and a target. The source point cloud is the point cloud corresponding to the initial state of the surface of the specimen even before being subjected to freezing and thawing loads. The 'intact' surface of the source point cloud is first extracted using the RANdom SAmple Consensus (RANSAC) algorithm for plane detection. Given the equation of the plane corresponding to this surface, a transformation matrix that aligns this surface to the co-ordinate axis is extracted using translation and rotation procedures. Figure 5 illustrates the concept of the individual steps of the determination of the transformation matrix.

In must be emphasized that at this point, the point clouds are not aligned but only the transformation matrix that aligns the reference surface to the co-ordinate axis is computed. Now, the target point cloud is aligned to the source point cloud by first removing the weathered surface from the scan by simply deleting the points below a certain z-coordinate value. These two partial scans are now aligned by first applying the global fast registration algorithm [18] followed by a local iterative closest point algorithm [19]. After local alignment, the transformation matrix is applied to both the source and target scans. A flowchart describing this procedure is shown in figure 8. Depending on the type of input file (source or target) the algorithm either generates the transformation matrix or starts the alignment process.

4.3. Data evaluation

The aligned scan data is subsequently cropped from the original sample surface size of approximately 150x110 mm^2 to a predefined format of 130x90 mm^2. This reduces each side by 10mm to remove the sample areas potentially exposed to a two-dimensional freeze-thaw attack. To ensure comparability between the temporal changes of the same

Preprints (www.preprints.org) | NOT PEER-REVIEWED | Posted: 28 November 2022 doi:10.20944/preprints202211.0507.v1

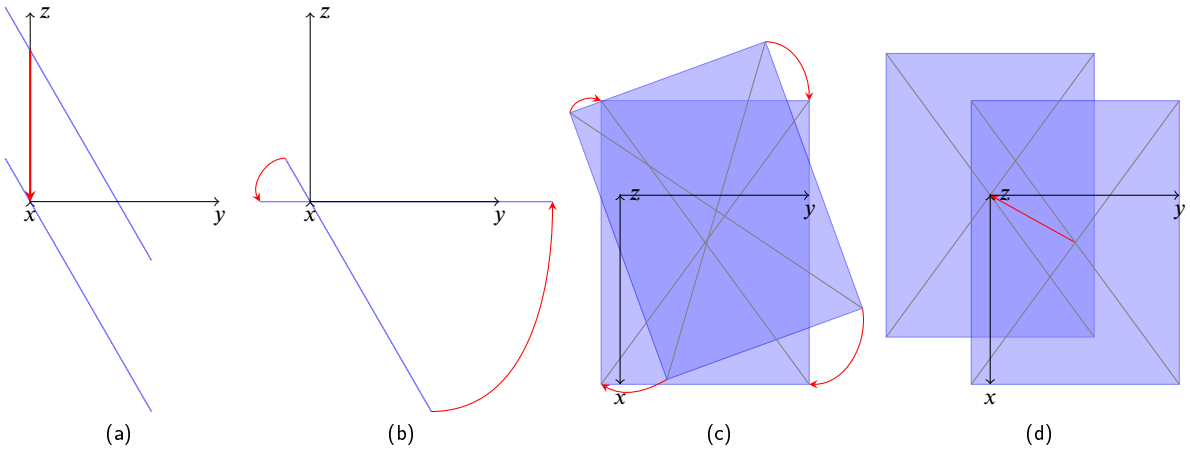

Figure 5: Subprocesses of determining the transformation matrix: (a) translation of the plane to the x-y plane, (b) rotation onto the x-y plane, (c) alignment with the x-y axes and (d) translation to the coordinate center.

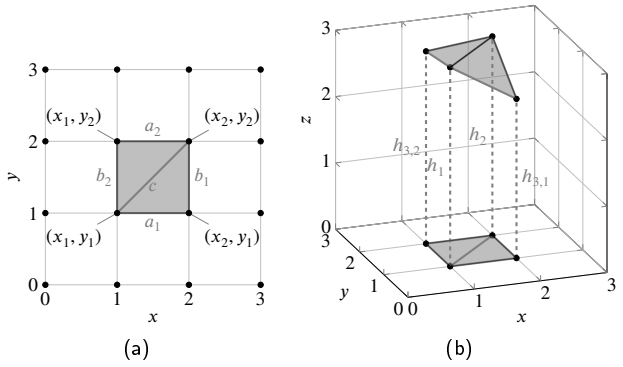

Figure 6: Concept of (a) generating two truncated triangular prisms for each grid segment and (b) illustrating a three-dimensional prism with varying z-axis coordinates.

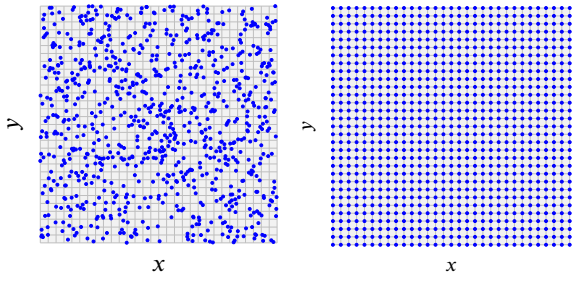

Figure 7: Concept of (a) unaligned scan data nodes and (b) x-y axis aligned mesh.

sample as well as different concrete mixture series, the three-dimensional coordinate nodes of the cropped sample data are aligned to the x-y coordinate grid with a linear nearest-neighbor approximation. This results in a uniform x-y orientation of every sample where only the z-axis coordinate varies. Figure 7 illustrates the original, unaligned scan data (blue nodes) in the x-y plane (a) and the aligned mesh after approximation (b).

The z-axis component of each node is mainly used for the subsequent data analysis processes.

4.3.1. *Sample volume and area*

In addition, the x-y-z grid also allows the calculation of the sample volume and area. The volume is calculated by constructing two truncated triangular prisms for each grid segment, see figure 6.

The volume of each prism is calculated according to equation 1:

$$V_k = \frac{1}{3} A_k (h_1 + h_2 + h_{3,k}), \forall k \in \{1, 2\} \tag{1}$$

where V_k is the volume of the truncated triangular prism, A_k is the base triangle area at $z = 0$ and h_1, h_2, h_3 are the heights of the prism corners.

Analogously, the sample surface area is calculated by adding up the two triangle areas of each grid segment. Each triangle area is calculated with three given side lengths according to the Heron's Formula, see equation 2:

$$A_k = \sqrt{s(s - a_k)(s - b_k)(s - c)}, \forall k \in \{1, 2\} \tag{2}$$

where A is the triangle area, s is the semi perimeter, $s = \frac{a+b+c}{2}$ and a_i, b_i are the triangle side lengths (mesh size). c is the hypotenuse length of right mesh triangle.

4.3.2. *Surface tortuosity*

The surface area data is used to calculate the tortuosity τ_i of the surface after i FTCs, see equation 3.

$$\tau_i = \left(\frac{A_i^{total}}{A_0^{total}} \right)^2 \tag{3}$$

Preprints (www.preprints.org) | NOT PEER-REVIEWED | Posted: 28 November 2022 doi:10.20944/preprints202211.0507.v1

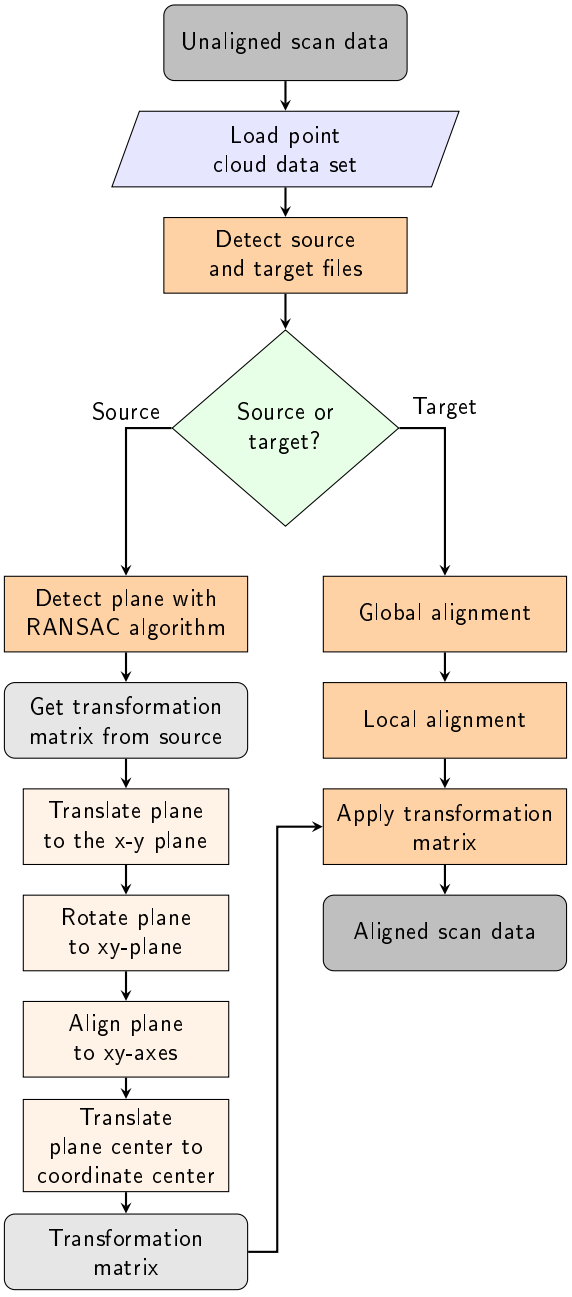

Figure 8: Flowchart of the alignment algorithm.

where A_i^{total} is the total surface area after i FTCs and A_0^{total} is the total surface area at 0 FTC. This two-dimensional toruosity can be interpreted as the roughness of the sample surface.

4.4. Comparison with CDF results

In order to compare the scan data results with the CDF results, the volume results are used to determine the mass loss of the samples. For this purpose, the volume difference of the the current freeze-thaw cycle and the volume before frost exposition is being divided by the density of the sample. The mass difference is then divided by the predefined scan surface area of 130x90 mm². This ultimately results in the surface weathering w_i in g/m², analogously to the CDF weathering results.

$$\Delta V_i^{total} = V_0^{total} - V_i^{total} \tag{4}$$

$$\Delta m_i = \Delta V_i^{total} \rho_i \tag{5}$$

$$w_i = \frac{\Delta m_i}{A_{scan}} \tag{6}$$

where ΔV_i^{total} is the volume difference, V_i^{total} is the volume of the sample, Δm_i is the mass difference, ρ_i is the density of the observed sample, w_i is the surface weathering from scan data after i FTCs. A_{scan} is the predefined scan data area of 130x90 mm² and V_0^{total} is the total volume of the sample at 0 FTC.

5. Results and discussion

The results presented in this paper are based on the testing sets shown in table 1. After the alignment and grid approximation processes, the resulting x-y axis aligned cropped scan data acts as the starting point for the data analysis. At this stage the data analysis consists of the following functionalities.

Figure 9 shows the progress of the weathering profile during the CDF test after certain freeze-thaw cycles (FTC) of sample set M1 20-65.

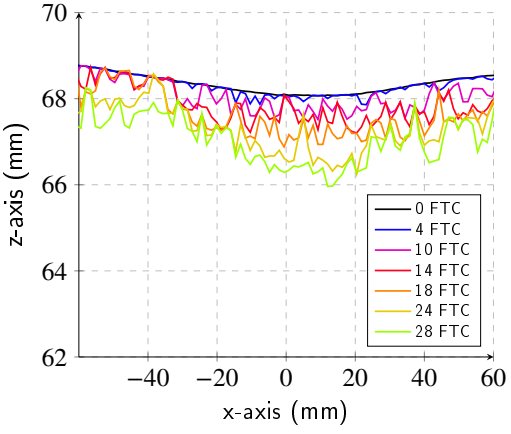

Figure 9: Variation of specimen cross section of sample set M1 20-65 as a function of FTC.

Both volume and surface area of each FTC scan are compared to the values of the reference scan. This results in the volume loss and tortuosity graphs, see figure 10. For samples with a high amount of weathering, the tortuosity of the sample set indicates an asymptotic curve approaching a specific maximum value (maximum roughness of the surface). The maximum roughness of the surface depends on the maximum aggregate size of the mixture.

Preprints (www.preprints.org) | NOT PEER-REVIEWED | Posted: 28 November 2022 doi:10.20944/preprints202211.0507.v1

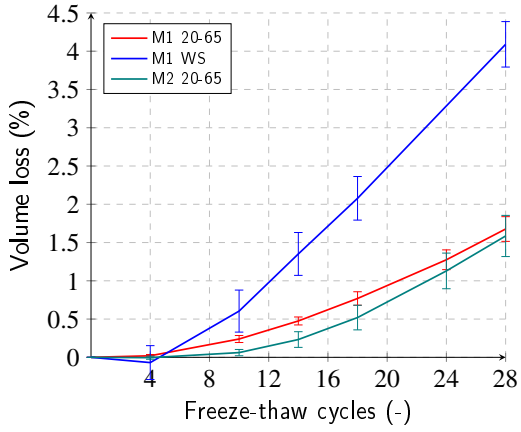

(a)

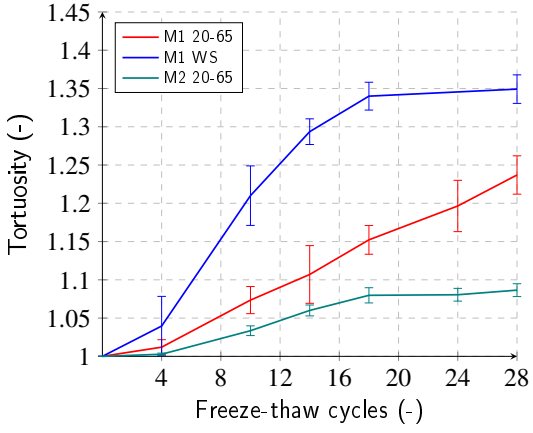

(b)

Figure 10: (a) Volume loss and (b) tortuosity of sample sets M1 20-65, M1 WS, and M2 20-65.

Both scan data weathering and CDF weathering of sample sets M1 20-65, M1 WS, and M2 20-65 are shown in figures 11, 12, and 13. It can be observed that both methodologies for the determination of the surface deterioration deliver comparable results (M1 20-65 and M2 20-65). For sample set M2-WS, where the surface damage is much higher compared to the aforementioned sample sets, the scan data weathering delivers lower results (6000 g/m²) compared to the CDF weathering (9000 g/m²).

Finally, figure 14 shows the correlation between the weathering results from both the standard CDF test and the scan data of all three sample sets. Sample sets M1 20-65 and M2 20-65 deliver a good correlation with R^2 scores of 0.98 and 0.94. In contrast, testing set M1 WS results in a weaker correlation with an R^2 score of 0.8175. The increased measured weathering from the CDF test is caused by an additional weathering effect on the vertical sides of the specimens due to isolation tape scaling.

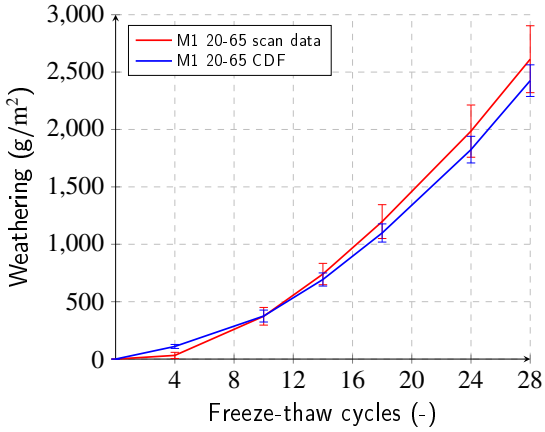

Figure 11: Scan data and CDF weathering results of sample set M1 20-65 in (g/m²).

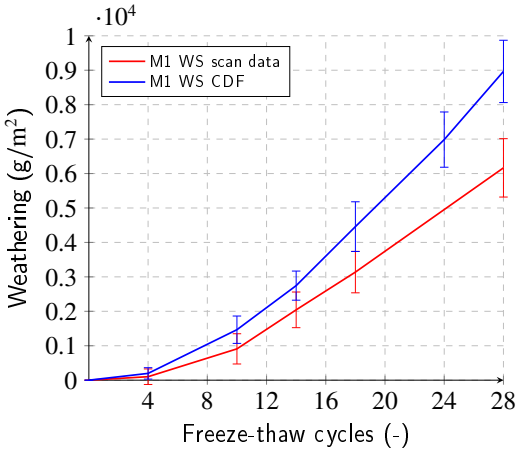

Figure 12: Scan data and CDF weathering results of sample set M1 WS in (g/m²).

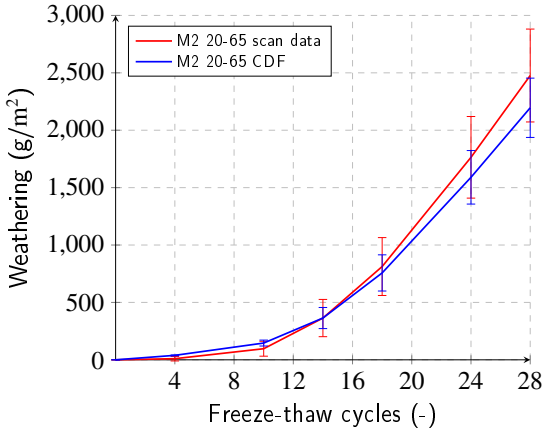

Figure 13: Scan data and CDF weathering results of sample set M2 20-65 in (g/m²).

Preprints (www.preprints.org) | NOT PEER-REVIEWED | Posted: 28 November 2022 doi:10.20944/preprints202211.0507.v1

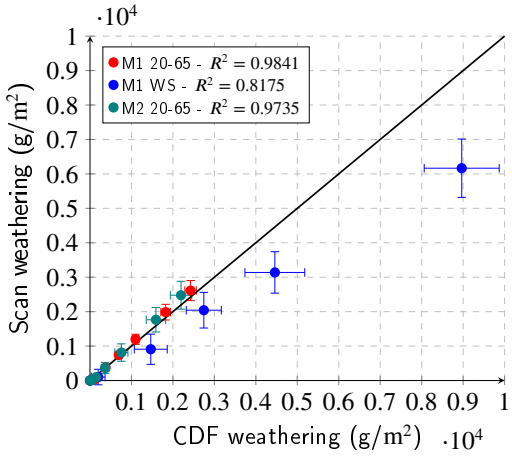

Figure 14: Correlation between weathering results from CDF and scan data in (g/m^2).

6. Conclusion

The methodology presented in this paper delivers new information regarding the surface deterioration of the CDF test samples and the associated distribution of the weathering depth. The results indicate a correlation between the progression of the distribution function and the sample's maximum aggregate size. This will be a subject for further investigations. The change of volume and area can be used to support the evaluation of the standard CDF methodology. Especially for sample sets with high amounts of weathering, it is suggested to consider the weathering results derived from the scan data. The underestimation of the material's performance due to additional weathering effects after tape scaling can be prevented using the 3D scanning methodology. Further investigations will be carried out regarding the presented 3D scan data characterization's use case and application for the evaluation of field experiment data.

References

[1] UN Department of Economic and Social Affairs Population Division. World urbanization prospects: The 2018 revision, 2018.

[2] Jochen Stark and Bernd Wicht. *Frost- und Frost-Tausalz-Widerstand von Beton*, pages 399–471. Springer Berlin Heidelberg, Berlin, Heidelberg, 2013.

[3] Susanne Palecki. *Hochleistungsbeton unter Frost-Tau-Wechselbelastung:-Schädigung- und Transportmechanismen*. Cuvillier Verlag, 2005.

[4] Treval C Powers, Llewellyn Everard Copeland, and HM Mann. Capillary continuity or discontinuity in cement pastes. Technical report, 1959.

[5] Max J Setzer. Micro-ice-lens formation in porous solid. *Journal of colloid and interface science*, 243(1):193–201, 2001.

[6] Treval C Powers and RA Helmuth. Theory of volume changes in hardened portland-cement paste during freezing. In *Highway research board proceedings*, volume 32, 1953.

[7] Olivier Coussy and Paulo J.M. Monteiro. Poroelastic model for concrete exposed to freezing temperatures. *Cement and Concrete Research*, 38(1):40–48, 2008.

[8] George W Scherer and JJ Valenza. Mechanisms of frost damage. *Materials science of concrete*, 7(60):209–246, 2005.

[9] George W Scherer. Freezing gels. *Journal of non-crystalline solids*, 155(1):1–25, 1993.

[10] Tingtao Zhou, Mohammad Mirzadeh, Roland J-M Pellenq, and Martin Z Bazant. Freezing point depression and freeze-thaw damage by nanofluidic salt trapping. *Physical Review Fluids*, 5(12):124201, 2020.

[11] Jithender J Timothy, Alexander Haynack, Thomas Kränkel, and Christoph Gehlen. What is the internal pressure that initiates damage in cementitious materials during freezing and thawing? a micromechanical analysis. *Applied Mechanics*, 3(4):1288–1298, 2022.

[12] Bundesanstalt für Wasserbau. BAW-Merkblatt Frostprüfung von Beton (MFB). 2012.

[13] Sampsa Kohtala, Jørgen F Erichsen, Ole Petter Wullum, and Martin Steinert. Photogrammetry-based 3d scanning for supporting design activities and testing in early stage product development. *Procedia CIRP*, 100:762–767, 2021.

[14] Abid Haleem, Pawan Gupta, Shashi Bahl, Mohd Javaid, and Lalit Kumar. 3d scanning of a carburetor body using comet 3d scanner supported by colin 3d software: Issues and solutions. *Materials Today: Proceedings*, 39:331–337, 2021.

[15] Robin H Helle and Hirpa G Lemu. A case study on use of 3d scanning for reverse engineering and quality control. *Materials Today: Proceedings*, 45:5255–5262, 2021.

[16] Behzad V Farahani, Francisco Barros, Mihai A Popescu, Pedro J Sousa, Paulo J Tavares, and Pedro Moreira. Geometry acquisition and 3d modelling of a wind tower using a 3d laser scanning technology. *Procedia Structural Integrity*, 17:712–717, 2019.

[17] Creaform. HandySCAN 3D | BLACK Series, 2022.

[18] Qian-Yi Zhou, Jaesik Park, and Vladlen Koltun. Fast global registration. In *European conference on computer vision*, pages 766–782. Springer, 2016.

[19] Szymon Rusinkiewicz and Marc Levoy. Efficient variants of the icp algorithm. In *Proceedings third international conference on 3-D digital imaging and modeling*, pages 145–152. IEEE, 2001.